Observations of the Sunyaev–Zel'dovich effect at high angular resolution towards the galaxy clusters A665, A2163 and CL0016+16

F.-X. Désert ^{a,b}, A. Benoit ^c, S. Gaertner ^e, J.–P. Bernard ^b, N. Coron ^b, J. Delabrouille ^{b,f}, P. de Marcillac ^b, M. Giard ^e J.–M. Lamarre ^b, B. Lefloch ^d, J.–L. Puget ^b, and A. Sirbi ^c

^dIRAM, avd Divina Pastora 7 Nucleo Central 18012 Granada Spain

Abstract

We report on the first observation of the Sunyaev–Zel'dovich (SZ) effect, a distortion of the Cosmic Microwave Background radiation (CMB) by hot electrons in clusters of galaxies, with the Diabolo experiment at the IRAM 30 m telescope. Diabolo is a dual–channel 0.1K bolometer photometer dedicated to the observation of CMB anisotropies at 2.1 and 1.2 mm. A significant brightness decrement in the 2.1 mm channel is detected in the direction of three clusters (Abell 665, Abell 2163 and CL0016+16). With a 30 arcsecond beam and 3 arcminute beamthrow, this is the highest angular resolution observation to date of the SZ effect. Interleaving integrations on targets and on nearby blank fields have been performed in order to check and correct for systematic effects. Gas masses can be directly inferred from these observations.

^aLaboratoire d'Astrophysique de l'Observatoire de Grenoble, 414 rue de la Piscine, BP 53, F-38041 Grenoble Cedex 9

^bInstitut d'Astrophysique Spatiale, Bât. 121, Université Paris XI, F-91405 Orsay Cedex France

^c Centre de Recherche sur les Très Basses Températures, 25 Avenue des Martyrs BP166, F-38042 Grenoble Cedex 9 France

^eCentre d'Études Spatiales sur les Rayonnements, 9 Avenue du Colonel Roche, BP 4346, F-31029 Toulouse Cedex France

f Enrico Fermi Institute, University of Chicago, 5460 South Ellis Avenue, Chicago, IL 60637, USA

1 Introduction

After the discovery of the Cosmic Microwave Background (CMB) radiation by Penzias & Wilson [33], and the observation of hot ionised gas in clusters of galaxies through its X-ray emission [43], Sunyaev & Zel'dovich [39] soon realised that the scattering of the CMB photons by the hot electrons of the intracluster medium (ICM) should generate a distinctive spectral distortion of the CMB blackbody spectrum in the (sub)millimetre and radio domain. Several millimetre and radio detections towards a dozen of clusters have recently been obtained using various techniques [8,9,13,29,42,25]. These results, which are compatible with the expected brightness decrement, constitute a direct evidence for the SZ effect and have profound cosmological importance:

- They are a strong confirmation of the cosmological origin of the CMB radiation.
- The mass of the ionised gas in clusters of galaxies can be obtained from SZ measurements, even for unresolved clusters [15]. If hydrostatic equilibrium is assumed, the total mass can also be deduced from the SZ profile, and compared with cluster mass estimates by other methods (gravitational lensing, velocity fields) for consistency. This, together with cluster number counts, yields an estimate of Ω at cluster scales.
- The detection via the SZ effect of very distant clusters ($z \simeq 1$ and above) would put severe constraints on Ω , as only in a low-density Universe could structures form so early (e.g. [3]).
- The angular diameter distance to a cluster can be estimated from the CMB intensity change due to the SZ effect combined with the observed X-ray surface brightness. For low redshift clusters, the combination of SZ and X-ray data thus allows estimating the Hubble constant H_0 [6,12,38]. For high redshift clusters, because of the additional dependence of the angular diameter distance on the deceleration parameter q_0 [38], it is also possible, in principle, to constrain Ω and Λ (see [30] for an application of the method to available SZ measurements).
- The measurement of the kinetic SZ effect on many clusters using an optimal filtering technique would make a measurement of very large scale velocity flows possible [24,1].
- The SZ effect is the strongest "contamination" source for the measurement of the primary CMB anisotropies at high angular resolution and in the millimetre spectral window, and therefore deserves careful studies (one's noise is the other's signal), especially in the light of the preparation to the Planck mission [5].

In an effort to detect the SZ effect in clusters at high redshift, we installed the Diabolo photometer at the focus of the IRAM 30 m millimetre radiotelescope (MRT). This photometer saw its first light (Benoit et al. [4]) at the Millimetre

Infrared Testa Grigia Observatory (MITO) in Italy on a 2.6 m telescope. The task of detecting a signal which is a part in a million of the background is very challenging but at a wavelength around 2 mm, the confusion by other astrophysical sources (dust, point sources, CMB anisotropies [19,18]) is minimal. In addition, the high angular resolution achieved with the 30 m facility (about 30 arcseconds for the two Diabolo channels) reduces the beam dilution on distant clusters. Owing to major improvements in bolometer and cooling technology, this task can now be achieved in a reasonable integration time (a few hours). The observations and data reduction method are described in section 2, and the results are presented and discussed in section 3.

2 Observations at the IRAM 30 m telescope

The Diabolo experiment is a dual—channel photometer of which the innovative cooling system, bolometers and readout electronics are prototypes for space submillimetre astronomical applications (the ESA Planck Surveyor mission [5] and FIRST cornerstone [34]). It is a cryostat with two bolometers observing around 1.2 and 2.1 mm, cooled to 0.1 K by a ${}^{3}\text{He}^{-4}\text{He}$ compact dilution fridge. The two bands matching the atmospheric windows are obtained with low pass filters common to the two channels and free-standing bandpass meshes after the light is selected by a dichroic beam splitter. The bolometer at 1.2 mm provides a constant monitoring of the so-called atmospheric noise in a coaligned and co-extensive beam with respect to the 2.1 mm "astrophysical" bolometer channel. The instrument, described in length by Benoît et al. [4], has been modified as follows for the present observations:

- Only one bandpass filter is used for the 2.1 mm channel, instead of two, in order to increase the detection efficiency. We checked that the small spectral leaks that appeared at high frequency have no influence on the SZ measurements.
- New readout electronics, now fully digital, have been used. Each bolometer is AC square—wave modulated in opposition in a Winston bridge with a stable capacity. The out-of-equilibrium voltage is amplified by a cold FET and warm amplifiers, AD converted, and then numerically demodulated after the electrical transients have been blanked. The digital signal is proportional to the total power received by the bolometer up to an arbitrary offset constant. A complete discussion of the readout electronics scheme can be found in [20].
- A NbSi thermometer has been installed on the dilution fridge to monitor the $100\,\mathrm{mK}$ cold base plate temperature. Another resistance used as a heater now allows an active regulation of this base plate temperature within about $30\mu\mathrm{K}$. This is especially useful for skydips (see Paragraph 2.1.4) and to avoid changes in the responsivity.
- A warm polyethylene lens (90% transmission) has been installed in front of

the cryostat to match the f-ratio of the telescope (about ten) with that of the instrument (about five).

The photometer has been installed at the Nasmyth focus of the telescope for a test run from November 10th to November 14th 1995, when the precipitable water vapor was too large (typically 5 to 9 mm) for sensitive measurements. The sensitivity and calibration of the instrument could nevertheless be measured on bright sources. Some 100 hours of observing time were allocated from December 1st to 4th from which the following results have been obtained. These observations were complemented with a few more hours in December 1996.

2.1 Calibration

2.1.1 Alignment

The alignment of the cryostat with respect to the telescope axes was achieved using a movable hot load situated between the entrance of the cryostat and the secondary. The recording of the signal in total power mode gives the beam direction and the appropriate corrections to be done for the cryostat optical axis to be pointed at the center of the secondary, which is crucial for straylight minimisation.

2.1.2 Pointing

Pointing corrections were made every two hours, using data obtained by scanning across a strong (several Jy) source (planet, quasar) situated near the target. The signal was modulated by the wobbling secondary at about 1 Hz. Fig. 1 shows the demodulated signal as a function of telescope direction along lines of constant elevation and constant azimuth. A Gaussian fit is made to determine pointing corrections if necessary.

2.1.3 The beam pattern

The beam pattern has been measured on Saturn in the November 95 test run with a simple azimuth-elevation mapping technique. It is shown in Fig. 2 for the two wavelengths. The beam centers (as defined by Gaussian one-dimensional fits) are within less than 2 seconds of arc from each other, confirming the accuracy of optical positioning of the two bolometers with respect to the system optical axis inside the cryostat. Fig. 3 shows the two integrated beam profiles as defined by the function of the angular radius θ starting from

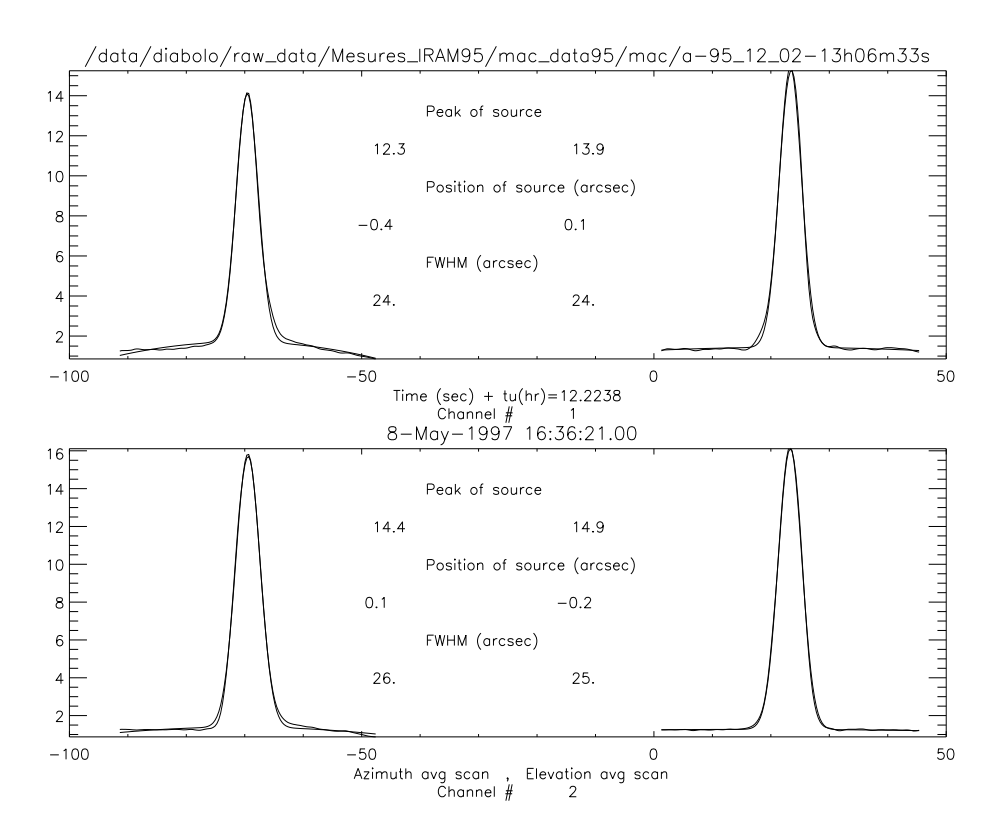


Fig. 1. The average demodulated signal from back and forth scans across Mars. The top and bottom panels are for the 1.2 mm and 2.1 mm channels respectively. For both panels, the left plot corresponds to a constant elevation scan, the right one to a constant azimuth scan. The X axis is in arcseconds, the Y axis is in μ V. A Gaussian fit is superposed to the data. Parameters of the fit are written on each panel. The precision on the center and FWHM is about 2 and 3 arcseconds respectively.

the center of the beam:

$$B(\theta) = \int_{0}^{\theta} d\theta' \, \theta' \int_{0}^{2\pi} d\phi \frac{S(\theta', \phi)}{S(0, 0)}, \qquad (1)$$

where the measured signal S is in cylindrical coordinates and where an off-set, estimated in the outskirts of the beam ($\theta > 45\,\mathrm{arcsec}$) has been taken out. B has units of a solid angle and represents the integrated beam efficiency which levels off at large θ . The beams for the two channels are much alike, except that the longer wavelength channel one is slightly more extended because of diffraction effects. Saturn is not point-like (17 arcsec diameter) and slightly distorts the real beams. The integrated beamwidth, calculated from the integrated beam solid angle $\Omega_{\rm mb}$ as $\theta = \sqrt{4\Omega_{\rm mb}/\pi}$ is larger than the one–dimensional Gaussian FWHM (34 instead of 25 arcseconds), because of near–sidelobe wings.

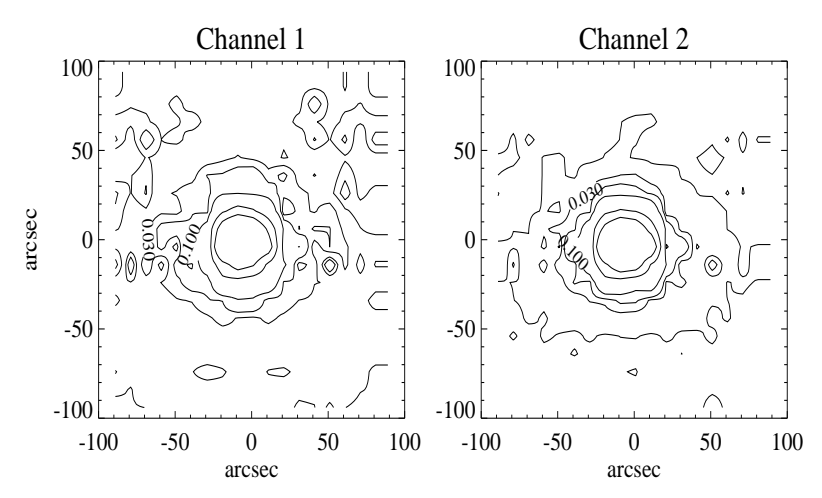


Fig. 2. Contour map of the two beams observed by mapping Saturn. Contour levels are at 0, 1, 3, 5, 10, 30, and 50% of peak value.

2.1.4 Skydips

Skydips must be performed in order to compare fluxes measured at different elevations β . If the optical depth at the zenith $\tau_0(\lambda)$ is known, all the measurements F can be put on the same scale "outside" the atmosphere, yielding corrected measurements F_c . Assuming a plane-parallel geometry, this can be written as:

$$F_c(\lambda) = F(\lambda) \exp\left(\frac{\tau_0(\lambda)}{\sin \beta}\right).$$
 (2)

Skydips were done in total power mode without any modulation, by having a scan of the whole telescope at constant azimuth through 10 steps of elevation with a constant cosecant increment. The skydip technique has been pionneered by Chini & Kreysa [14] at the IRAM 30 m telescope. Here, we did not need a chopper for reference. The signal S_i in a given channel and at elevation β_i , for an average atmospheric temperature T_{atm} , can be written as:

$$S_i = C + B_f T_{atm} \left(1 - \exp\left(-\frac{\tau_0}{\sin \beta_i} \right) \right). \tag{3}$$

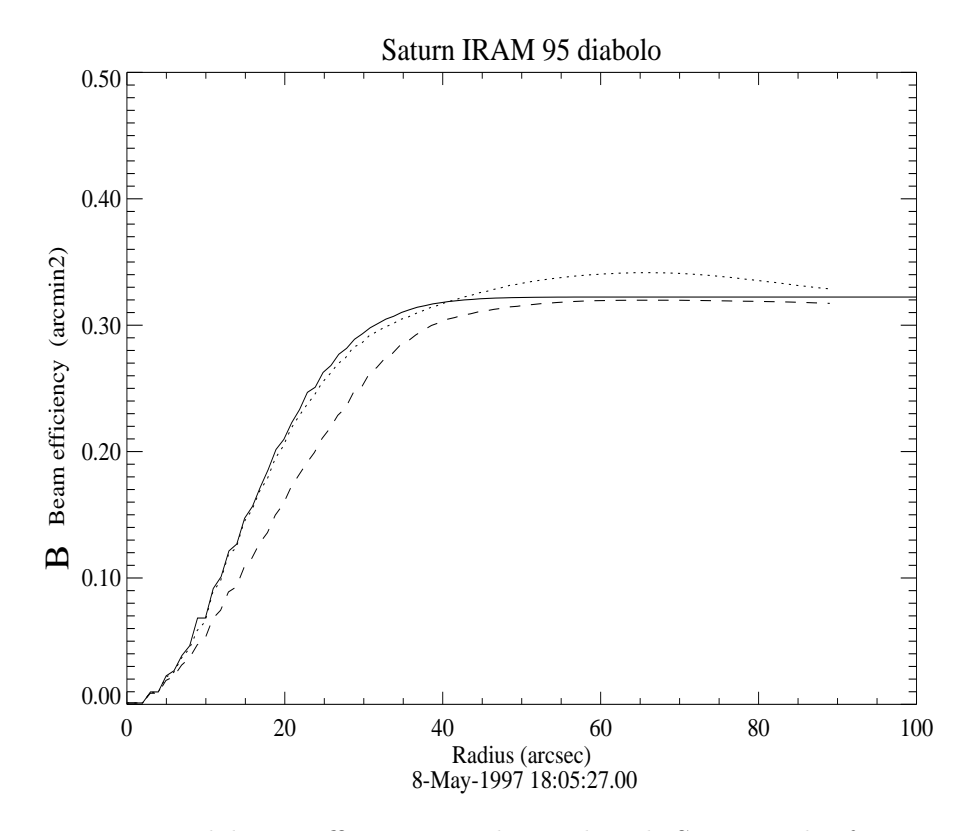


Fig. 3. Integrated beam efficiency as observed with Saturn. The function $B(\theta)$ defined by Eq. 1 is plotted for the two wavelengths (dotted line for 1.2 mm and dashed line for 2.1 mm) against the angular radius θ . The simulated integrated beam of a 2-dimensional Gaussian of FWHM 34 arcsecond convolved with the Saturn 17 arcsecond disk is shown as a plain line.

At each wavelength (1.2 and 2.1 mm), the constant C represents an arbitrary zero level. The forward beam efficiency $B_f = dS/dT$ is compared to the main beam efficiency B_m (see below Paragraph 2.1.5). Before formula 3 can be applied, one has to correct for the drifts of the 100 mK base plate temperature T_{bath} , induced by the increasing heat load that occurs with the skydip. The NbSi thermometer gives a sufficiently sensitive measurement of T_{bath} . With a simple linear correlation technique, the coefficients of which are established independently of the skydip, the contribution $dS/dT_{bath} \times T_{bath}$ can be subtracted. Fig. 4 shows the non-linear fit of the data based on formula 3. The correction which is applied to the data via Eq. 2 is deduced by interpolating between the two observed skydip values of $\tau_0(1.2 \text{ mm})$ closest in time to the observation. It is found to be only of the order of 30% or less at 2.1 mm where the SZ effect is expected. During the December 95 observations, the zenith optical depths at 1.2 mm varied between 0.1 and 0.3, which corresponds to 2-4 mm of precipitable water vapour. This definitely is an acceptable range of opacity values for SZ measurements.

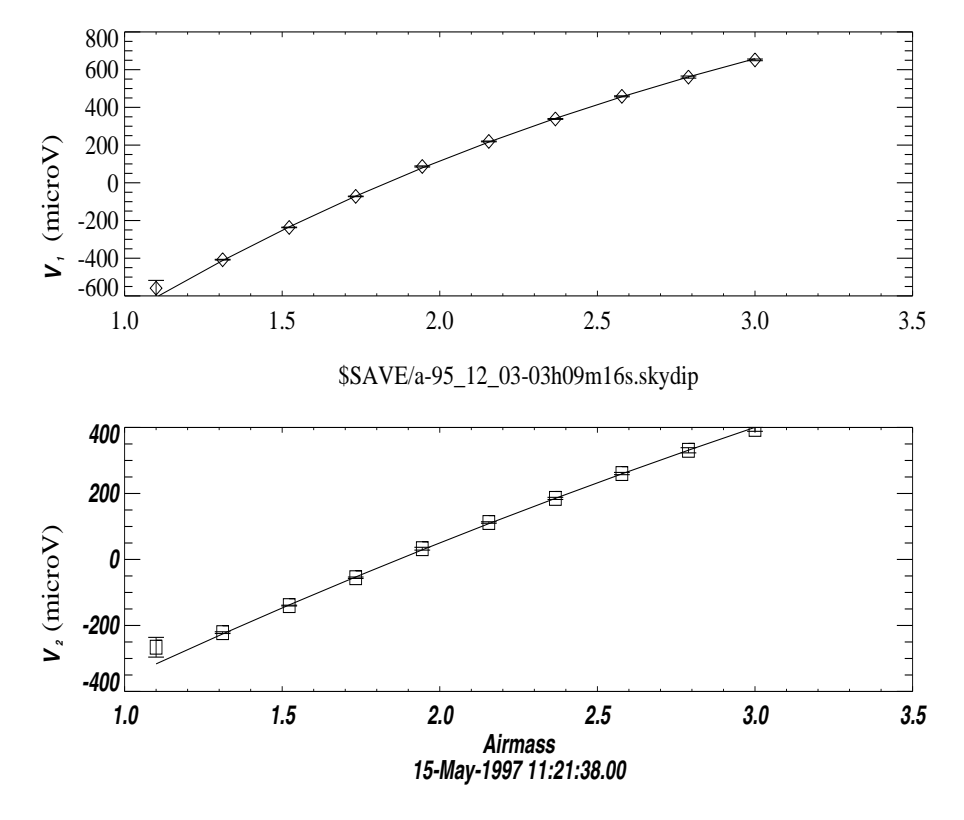


Fig. 4. Total power skydip measurements for the 2 channels. The average signal output in μV as a function of airmass is fitted using the model of Eq. 3.

2.1.5 Sensitivity

The calibration is done with planets which partially fill the beam. Mars (angular diameter 4.1 arcsec.), Saturn (16.7 arcsec.) and Jupiter (30.5 arcsec.) have been used for the present observations assuming a blackbody emission with temperatures of respectively 214, 150, and 170 K. After correcting for atmospheric opacity effects (Eq. 2), and taking into account the beam dilution, the responsivity of each bolometer $B_{mc}(\lambda) = dS/dT$ is deduced. It represents the response of the bolometer to 1 Rayleigh-Jeans Kelvin filling the main beam. The noise level is measured on blank fields. The instrument noise on the sky was found to be above the bolometer noise (as measured in the laboratory) by a factor of 3. The additional noise is likely related to an imperfect isolation from vibrations in the Nasmyth cabin, which generates noise of microphonic origin by optical modulation of straylight.

The final sensitivities are given in Table 1, when the sky noise is minimal and the zenith opacity is 0.1 at 1.2 mm. FWHM is given by the point source profile Gaussian fit and $\Omega_{\rm mb}$ is the integrated beam solid angle up a 45 arcseconds radius. Brightness sensitivities are for a filled beam, and flux sensitivities are for a point source on axis. These best performances are degraded whenever the source is not at the zenith, the sky is less transparent or the sky is more noisy. The overall noise degradation can be by as much as a factor of 3 at

Table 1
Best sensitivities obtained with Diabolo at the IRAM 30 m telescope in 1995. Sensitivities in parentheses are for the 2.1 mm channel after spectral decorrelation of the atmospheric noise (see text).

Channel	FWHM arcsec.	$\sqrt{\frac{4\Omega_{\mathrm{mb}}}{\pi}}$ arcsec.	$mK.s^{1/2}$	$MJy sr^{-1}.s^{1/2}$	$mJy.s^{1/2}$
$1.2\mathrm{mm}$	24 ± 3	34 ± 2	25	50	900
$2.1\mathrm{mm}$	27 ± 3	34 ± 2	13(11)	8(7)	170(140)

1.2 mm, but rarely exceeds fifty percent at 2.1 mm. In all cases, sky noise can be reduced by a decorrelation technique (see Section 3). The corresponding noise levels are given in parentheses in Table 1. For the observation technique described in section 2.2, the effective sensitivity is worse than in Table 1 by a factor of 2.

The ratio between the corrected main beam efficiency $B_{mc}(\lambda)$ (obtained from mapping planets) and the forward beam efficiency $B_f(\lambda)$ (obtained from skydips: Eq. 3) is only 25% ± 5 (50% ± 5) at 1.2 (resp. 2.1) mm. These values are in agreement with the telescope efficiencies measured by Garcia-Burillo et al. [21]. The far sidelobe pattern implied by these results can be troublesome for the observation of weak sources. This question is addressed in the discussion of Section 3.

2.2 Observing strategy

Four types of modulation were simultaneously used in order to limit the various low–frequency noises and monitor systematics.

- (1) The electronic AC modulation, referred to in the beginning of this section, avoids using electronics at frequencies below $10 \,\mathrm{Hz}$ (the typical 1/f knee frequency). Here we modulate the bolometers at $36 \,\mathrm{Hz}$ and the readout electronics deliver one sample per bolometer at the rate of $72 \,\mathrm{Hz}$.
- (2) The wobbling secondary provides the second modulation at the typical frequency of 1 Hz and with a beamthrow of 3 arc minutes. This allows the slowly varying background emission (sky and telescope) to be subtracted from the comparison of the on-axis measurement with that from an offset position at the same elevation.
- (3) The whole telescope is nodded in azimuth every 20 seconds with an amplitude of 3 arcminutes in an ABBA cycle which is repeated 4 times to

- form one scan. This permits to compensate for any imbalance between the two beams provided by the wobbling. Each scan obtained in this way lasts about 2 minutes (repointing overheads included).
- (4) Each scan above is done consecutively on a reference field offset from the target by a lag of a few minutes of time in RA (R at coordinates $(\alpha \log, \delta)$), on target twice (T and T' at coordinates (α, δ)), and on a second reference field offset by the same number of minutes of time in RA in the other direction (R' at coordinates $(\alpha + \log, \delta)$). With this method, the reference fields are followed in the same way as the target in local coordinates. This ensures that sidelobe effects (ground pickup), if any, are subtracted. This technique has been used by Herbig et al. [25] for single-dish measurements of very weak sources with proper baseline subtraction.

2.3 Reduction procedure

The data reduction proceeds as follows.

- (1) Cosmic ray hits are removed by interpolation from the data flow by a running median algorithm. Typical time constants are 10 milliseconds and the glitch rate is less than one hit per bolometer every 10 seconds, so that few samples are affected. The particles which deposit their energy into the bolometer are thought to mainly be muons, more abundant at the telescope site than in the laboratory.
- (2) The data are then synchronously demodulated with the help of the wobbler position (which is recorded along with the bolometer signals). The mean and dispersion values are computed for each position of the nodding cycle *ABBA*. Typical offsets (the imbalance between the positive and negative wobbler positions) are of the order of 0.2 K.
- (3) A complete scan is reduced by averaging the differences of values between the two nodding positions: $v = \sum_{1}^{N} (v_A v_B)/(2N)$. The noise on the final value is obtained from the dispersion of the individual differences. The sensitivity quoted in Table 1 corresponds to the best noise figure obtained after a scan and corrected for the square root of the scan integration time.
- (4) The third channel, which is a thermometer measuring the base plate temperature $v_3 = T_{bath}$, is treated the same way as the two others in order to check for a possible systematic effect or additional noise possibly induced by drifts of the thermal bath temperature. None have been found.
- (5) A linear combination of the first two bolometers, $v_4 = v_2 rv_1$ is calculated. The ratio r is chosen so as to minimise the noise of v_4 . It can be shown that r can be deduced from a simple linear correlation between v_1 and v_2 even if both measurements are noisy, and r is always smaller than the color of the sky emission. This procedure is intended to specifically

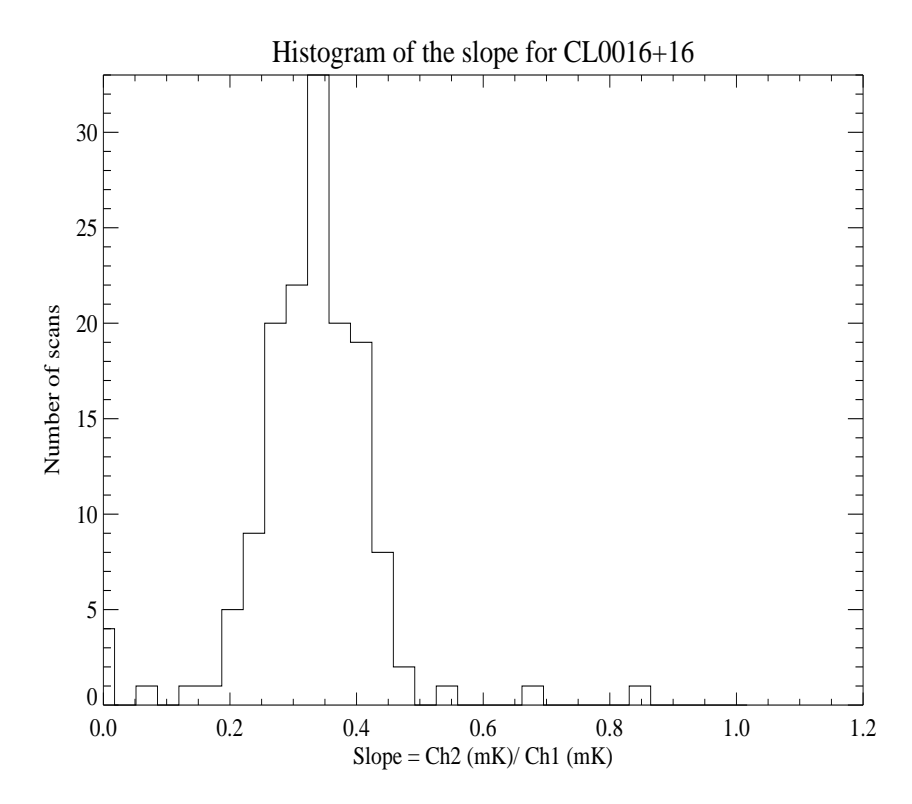


Fig. 5. Histogram of the values r, the slope between channel 2 against channel 1 in units of a temperature brightness ratio. A value of 0.3 is expected from the fluctuations of water vapour and the photometric model of the instrument. Sky noise seems indeed to be the source of extra noise seen in the bolometers.

work at removing sky noise from the second channel when little or no signal is expected from the first one (in particular, in case of the SZ effect). An histogram of the values of r during the December observations is shown in Fig. 5. The correlation coefficient C tells us by how much we can reduce the initial noise of v_2 to that of v_4 : $\sigma_4 = \sigma_2 \sqrt{1 - C}$. The typical correlation coefficient C of 0.4 leads to a small improvement in the signal to noise ratio of weak sources. On the other hand the statistical distribution which is obtained with the corrected v_4 is much closer to Gaussian than that of the data for the original channels, v_1 and v_2 (see 3.1).

(6) For each channel, an elementary block of data, made of 4 scans (R, T, T', R'), is reduced by computing an average signal $s = (v_T + v_{T'} - v_R - v_{R'})/2$ and a difference signal $d = (v_{T'} - v_T - v_R + v_{R'})$ with associated errors.

Four rich clusters of galaxies (A665, A2163, A2218 and CL0016+16) have been selected for observations due to their small angular core radius (less than 2 arcminutes), adapted to a large millimetre antenna. In addition to the 1995 data, we gathered a few more hours of observation towards two of these clusters (A2163 and CL0016+16) in 1996. The observation and data reduction schemes were very different, in an attempt to measure SZ profiles.

3 Tentative detections of the SZ effect

3.1 Results

The parameters of the observations towards the four clusters are given in Table 4, and the full results are summarised in Table 5 and 6 (antenna Rayleigh-Jeans equivalent temperature in μ K, corrected for atmospheric absorption). Rayleigh-Jeans temperature differences (the corrected signal s see 2.3) for all cycles of measurements are plotted in Fig. 6 to Fig. 9.

For the 1995 data, the final result for each cluster has been obtained by averaging the measurements obtained from each cycle of four scans, weighted proportionally to the inverse square of the noise for the individual sets. For each measurement, we compare the internal error obtained with this optimal averaging by using the internal noise value, and the external error obtained from the dispersion between the scan values. The square of the ratio between the two is the reduced χ^2 . The values listed in Tables 5 and 6 show the internal consistency of the measurement and its estimated noise, except for the first channel where the χ^2 value is systematically larger than unity. This discrepancy can be explained by the statistics of the atmospheric noise, which is not Gaussian and affects more the 1.2 mm channel than the 2.1 mm one. To first order, it should not affect much the decorrelated channel, as observed.

For the 1996 data, which use a different scanning technique, results have been obtained from the difference between the average of the signal from the scans on 30 arcseconds centered on the target source and the average value of the signal at more than 40 arcseconds of the target.

A significant negative signal is detected in the 2.1 mm decorrelated channel for the three clusters A665, A2163 and CL0016+16. This detection is particularly significant for the latter cluster.

If we interpret those measurements as due to the Sunyaev-Zel'dovich effect, one can convert the obtained value from antenna temperature to the y parameter (see [39,40]), neglecting the spectral dependency on the cluster gas temperature ([36,22]). The final results (1995, 1996, and combination of the two years) are given in Table 2.

The correction η for the 1995 beam dilution is calculated by convolving the measured beam profile obtained on Saturn (modulated at 3 arcmin) with a theoretical SZ profile using core parameters from X-ray measurements.

We do not detect any significant signal in the blank field positions $(v_R+v_{R'})$: in contrast to cm radio observations, no systematic signal is seen in the blank field

Table 2
Final calibrated results

		1995	1996	all	
Cluster	η	$y_0 / 10^{-4}$	$y_0 / 10^{-4}$	$y_0 / 10^{-4}$	S/N
A665	0.498	2.92 ± 1.15		2.92 ± 1.15	2.5
A2163	0.548	4.99 ± 1.97	4.60 ± 2.00	4.80 ± 1.40	3.4
A2218	0.607	-0.37 ± 2.21		-0.37 ± 2.21	0.2
CL0016+16	0.668	3.30 ± 0.90	2.90 ± 1.60	3.20 ± 0.78	4.1

Table 3 Physical parameters of the observed clusters taken from [9,17,10,32,26]. The total gas mass is computed from the present measurements. Uncertainties are statistical only.

Cluster	z	$T_e (\mathrm{keV})$	θ_c arcmin	β	$Y (10^{-4} \operatorname{arcmin}^2)$	$M_g/10^{14}M_{\odot}$
A665	0.182	8.2	1.60	0.66	439	20.2 ± 8.0
A2163	0.201	14.6	1.20	0.62	491	14.6 ± 4.2
A2218	0.171	6.72	1.00	0.65	< 408	$< 20.9 (3\sigma)$
CL0016+16	0.541	8.22	0.64	0.68	70	11.1 ± 2.7

measurements. Indeed, we find that the average signal obtained by keeping only the on-source component $(v_T + v_{T'})$ is about $\sqrt{2}$ more significant than that shown in Tables 5 and 6. This gives us confidence in the final results for the y parameters of Table 2. Moreover, for A2163 and CL0016+16, the 1995 and 1996 results are compatible with each other.

An additional outcome of the observations are temperature differences from blank field measurements (d: see 2.3). No signal is detected in any of the 4 differences (around the 4 observed clusters) at the $\Delta T/T = 2 \times 10^{-4}$ level (1σ). If this result were improved by repeated measurements on a larger number of clusters, it could yield interesting constraints on the level of CMB anisotropies at small angular scales (30 arcseconds to few arcminutes) in a wavelength range where the smallest contamination from radio and infrared galaxies [19] is expected.

All clusters show no signal at 1.2 mm within the observational errors. In principle, both the thermal and kinetic SZ effect could contribute to this channel, but the upper limit that we can put on cluster radial velocities is not stringent enough to be relevant. No galactic dust emission is detected either.

3.2 Interpretation

The mass of hot gas can be directly deduced from these observations by using:

$$M_g = 8.2 \times 10^{14} M_{\odot} \left(\frac{h}{0.5}\right)^{-2} \left(\frac{Y}{10^{-4} \,\mathrm{arcmin}^2}\right) \left(\frac{kT_e}{10 \,\mathrm{keV}}\right)^{-1} \frac{(\sqrt{1+z}-1)^2}{(1+z)^3},\tag{4}$$

a formula derived by De Luca et al. [15]. Here we have assumed $\Omega_0 = 1$ and $h = H_0/(100 \, \mathrm{km/s/Mpc})$, and the measurement y_0 has been converted into $Y = \int y d\Omega = y_0 \Omega_{\mathrm{eff}}$. The effective solid angle Ω_{eff} is calculated with

$$\frac{\Omega_{\text{eff}}}{\theta_c^2} = f_{\text{geom}} = 2\pi \int x dx (1 + x^2)^{\frac{(1-3\beta)}{2}},$$
(5)

and $x = \theta/\theta_c$, assuming a King profile with an angular core radius of θ_c . The resulting masses are given in Table 3. Parameters for the clusters, θ_c , β , and T_e , have been taken from recent ROSAT X-ray measurements. These estimated masses do not depend on the absolute X-ray fluxes.

Our result for A2163, $y_0 = 4.8 \pm 1.4 \times 10^{-4}$ is in agreement with the determination by Wilbanks et al. [42] of $y_0 = (3.78^{+0.74}_{-0.65}) \times 10^{-4}$ and that of Holzapfel et al. [28] of $y_0 = (3.73^{+0.47}_{-0.61}) \times 10^{-4}$, both obtained at the same wavelength (2.1 mm) as the present measurements with the 1.4' beam (2' throw) of the SuZie experiment. It is also in agreement with the submillimeter detection by the SPM photometer onboard the PRONAOS balloon (with a 3.7' beam and 6' beamthrow). A detailed discussion of the combined bolometer results for A2163 is given by Lamarre et al. [31]. The gas mass we deduce is $14.6 \pm 4.2 \times 10^{14} M_{\odot}$, very close to the X-ray determined gas mass [17] $14.3 \pm 0.5 \times 10^{14} M_{\odot}$.

Our most significant detection (at the 4 σ level) concerns the distant cluster CL0016+16 at a redshift of 0.541. This cluster is the highest redshift object detected with the SZ effect in the millimetric domain. Our result of $y_0 = 3.20 \pm 0.78 \times 10^{-4}$ is larger than but compatible with the central parameter $y_0 = 2.18 \times 10^{-4} (h/0.5)^{-1/2}$ predicted by Birkinshaw [11] using ROSAT X-ray data (within 1.3 σ). It is in agreement with the SZ radio determination of Hughes and Birkinshaw [27] with a larger beam (1.8' with a 7' beam throw) of $y_0 = 2.20 \pm 0.37 \times 10^{-4}$ (see also [8]), and more marginally with the SZ map of the interferometer experiment of Carlstrom et al. [13] of $y_0 = 1.31 \pm 0.12 \times 10^{-4}$, which spans 1 to 10' angular scales. Our gas mass estimate of

 $M_g = 11.1 \pm 2.7 \times 10^{14} M_{\odot}$ is twice as large as the X-ray gas mass deduced by Neumann and Böhringer [32] but still within errors.

For A665, the observations were centered on the IPC X-ray center as given by Birkinshaw, Hughes & Arnaud [9], which is offset by 2' from the nominal Abell center. Although less significant, the measured central brightness decrement $y_0 = 2.92 \pm 1.15 \times 10^{-4}$ is in agreement with the more accurate value $1.69 \pm 0.15 \times 10^{-4}$ determined by Birkinshaw et al. [9], albeit in the radio domain.

The integration time was clearly insufficient for A2218 to reach a significant noise level for that cluster. The upper limit that we get is compatible with the radio measurements that were previously reported [8,29].

3.3 Perspective

We have reported here the highest angular resolution (30") observations of the SZ effect on at least 2 clusters. These observations could be achieved thanks to the large millimetre Pico Veleta antenna and a total on source integration time of fifty hours. It is clear that SZ profiles or even maps of rich clusters can be measured with the Diabolo instrument, with sufficient winter integration time, when improvements in the overall efficiency are made (these are currently underway). These observations are complementary to X-ray measurements in the sense that they directly sample the gas pressure with similar angular resolution (the future XMM and AXAF will have few arcsecond resolutions). High resolution SZ observations in the millimeter atmospheric windows will also grow in importance after the unbiased survey of SZ clusters from the Planck Surveyor satellite. For resolved clusters the amplitude of the SZ distortion is independent of distance, and thus high-redshift clusters are adequate targets for millimetre observations of the SZ effect, whereas X-ray measurements of gas masses are more difficult.

Acknowledgements

We wish to thank the IRAM staff especially for their help during the setup of the instrument, Bernard Fouilleux for his help during the observations, and Bernard Lazareff for his support of the mission. We thank the whole Diabolo team for the continuous improvements brought to the instrument, with a special attention to Jean-Pierre Crussaire, Gerard Dambier, Jacques Leblanc, Bernadette Leriche, and Marco De Petris along with the Testa Grigia MITO team for a previous test of the instrument. INSU, IAS, CESR, CRTBT, and the GdR Cosmologie contributed financially to this instrument.

Table 4 Observation Logbook Summary

Cluster	RA (1950)	Dec (1950)	Offset (arcsec)	Int. time 95 (96)
A665 Source	08.26.25.0	+66.01.21.	0.	13.1 hours
A665 Ref1	08.25.29.2	+66.01.21.	-340.	
A665 Ref2	08.27.20.8	+66.01.21.	+340.	
A2163 Source	16.13.05.8	-06.01.29.	0.	5.7(3.2)
A2163 Ref1	16.13.05.8	-06.01.29.	-340.	
A2163 Ref2	16.13.05.8	-06.01.29.	+340.	
	<u></u> .			
A2218 Source	16.35.35.0	+66.18.50.	0.	3.1
A2218 Ref1	16.29.50.8	+66.18.50.	-2074.	
A2218 Ref2	16.41.19.2	+66.18.50.	+2074.	
CL0016+16 Source	00.15.58.3	+16.09.37.	0.	15.7 (9.8)
CL0016+16 Ref1	00.15.34.7	+16.09.37.	-340.	
CL0016+16 Ref2	00.16.21.9	+16.09.37.	+340.	
CL0016+16 Ref1p	00.10.18.2	+16.09.37.	-4900.	
CL0016+16 Ref2p	00.21.38.4	+16.09.37.	+4900.	

References

- Aghanim, N., De Luca, A., Bouchet, F. R., Gispert, R. and Puget, J.-L., 1997, A&A, 325, 9
- [2] Andreani, P., Pizzo, L., Dall'Oglio, G., et al. 1996, ApJL, 459, L49
- [3] Barbosa, D., Bartlett, J. G., Blanchard, A. and Oukbir, J., 1996, A&A, 314, 13

- [4] Benoît A., Zagury, F., Coron, N., et al. 1998, A&A Suppl.Ser., to be submitted
- [5] Bersanelli, M. et al., 1996, COBRAS/SAMBA: Report on the Phase A Study, ESA report D/SCI(96)3.
- [6] Birkinshaw, M., 1979, MNRAS, 187, 847
- [7] Birkinshaw, M., Gull, S. F., & Moffet, A. T. 1981, ApJL, 251, L69
- [8] Birkinshaw, M., 1991 in Proc. of *Physical Cosmology*, J. Trân Than Vân, ed., (Frontieres:Gif-sur-Yvette)
- [9] Birkinshaw, M., Hughes, J. P., & Arnaud, K. A. 1991, ApJ, 379, 466
- [10] Birkinshaw, M., & Hughes, J. P., 1994, ApJ, 420, 33
- [11] Birkinshaw, M., 1998, Physics Reports, in press
- [12] Cavaliere, A. and Danese, L. and De Zotti, G., 1979, A&A, 75, 322
- [13] Carlstrom, J. E., Joy, M., & Grego, L., 1996, ApJL, 456, L75
- [14] Chini, R., Kreysa, E., Mezger, P. G., & Gemuend, H.-P. 1986, A&A, 154, 8
- [15] De Luca, A., Désert, F.-X., and Puget, J.-L. 1995, A&A, 300, 335
- [16] Donahue, M., et al., submitted to ApJ (astro/ph 970710)
- [17] Elbaz, D., Arnaud, M., & Böhringer, H. 1995, A&A 293, 337
- [18] Fischer, M. L., & Lange, A. E., 1993, ApJ, 419, 433
- [19] Franceschini, A., De Zotti, G., Toffolatti, L. et al., 1991 A&AS, 89, 285
- [20] Gaertner, S., Benoit, A., Lamarre, J.-M. et al. 1997, A&AS, 126, 151
- [21] Garcia-Burillo, O. S., Guelin, M., & Cernicharo, J., 1993, A&A, 274, 123
- [22] Giard, M., 1995, "Proceedings of the XVth Moriond Astrophysics meeting", J. Tran Thanh Van eds., éditions Frontières.
- [23] Grainge, K., Jones, M., Pooley, G., Saunders, R., & Edge, A. 1993, MNRAS, 265, L57
- [24] Haehnelt, M., 1996, in "Proceedings of the XVIth Moriond Astrophysics meeting", F.R Bouchet, R. Gispert, B. Guiderdoni and J. Tran Thanh Van eds., éditions Frontières.
- [25] Herbig, T., Lawrence, C. R., Readhead, A. C. S., & Gulkis, S. 1995, ApJL, 449, L5
- [26] Hughes, J. P., Birkinshaw, M., & Huchra, J. P., 1995, ApJ, 448, L93
- [27] Hughes, J. P., & Birkinshaw, M., 1998, ApJ, submitted
- [28] Holzapfel, W., Arnaud, M., Ade, P. A. R., et al., 1997, ApJ, 480, 449

- [29] Jones, M., Saunders, R., Alexander, P., et al. 1993, Nature, 365, 320
- [30] Kobayashi, S., Sasaki, S., Suto, Y., 1996, Publ. Astron. Soc. Jap., 48, L107
- [31] Lamarre, J.-M., Giard, M., Pointecouteau, E. et al., 1998, ApJL, in press
- [32] Neumann, D. M., & Böhringer, H., 1997, MNRAS, 289, 123
- [33] Penzias, A. A., Wilson, R. W., 1965, ApJ, 142, 419
- [34] Pillbratt, G., 1997, in Proceed. of the ESA Symp. "The Far Infrared and Submillimetre Universe", ESA SP-401, 7
- [35] Pizzo, L., Andreani, P., Dall'Oglio, G. et al. 1995, Experim. Astron., 6, 249
- [36] Rephaeli, Y., 1995, ARA&A, 33, 541
- [37] Saunders, R., 1995, Ap. Lett. Comm., 32, 339
- [38] Silk, J. and White, S., 1978, ApJ, 226, L103
- [39] Sunyaev, R. A., & Zel'dovich, Ya. B., 1970, Ap. Sp. Sci., 7, 3
- [40] Sunyaev, R. A., & Zel'dovich, Ya. B., 1980, MNRAS, 190, 413
- [41] White, S. D. M., Silk, J., & Henry, J. P. 1981, ApJL, 251, L65
- [42] Wilbanks, T. M., Ade, P. A. R., Fischer, M. L., Holzapfel, W. L., & Lange, A. E. 1994, ApJL, 427, L75
- [43] Lea, S. M., Silk, J., Kellogg, E., Murray, S., 1973, ApJL, 184, L105

Table 5 Observation results

Channel	$\lambda(\mathrm{mm})$	Signal (μ K) (noise)	$\chi^2 (df)$	Prob %
A665				
source - ref (microK RJ):				
1	$1.2\mathrm{mm}$	193. (235. 277.)	41.6 (30)	7.7
2	$2.1\mathrm{mm}$	-224. (115. 129.)	37.7(30)	15.9
4	$2.1\mathrm{mm}$ corr	-253. (100. 106.)	33.7 (30)	29.3
ref2 - ref1 (microK RJ): $_$				
1	$1.2\mathrm{mm}$	-439. (470. 685.)	63.8 (30)	0.0
2	$2.1\mathrm{mm}$	-80. (231. 298.)	50.0 (30)	1.2
4	$2.1\mathrm{mm}$ corr	303. (200. 265.)	52.8 (30)	0.6
A2163				
source - ref (microK RJ):		-		
1	$1.2\mathrm{mm}$	-451. (398. 656.)	32.6 (12)	0.1
2	$2.1\mathrm{mm}$	-695. (247. 246.)	11.9 (12)	45.4
4	$2.1\mathrm{mm}$ corr	-476. (188. 203.)	14.1 (12)	29.6
ref2 - ref1 (microK RJ): _				
1	$1.2\mathrm{mm}$	-1388. (797. 1282.)	31.1 (12)	0.2
2	$2.1\mathrm{mm}$	961. (494. 657.)	21.2 (12)	4.7
4	$2.1\mathrm{mm}$ corr	636. (376. 405.)	13.9 (12)	30.6

Table 6 Observation results: following

Channel	$\lambda(\mathrm{mm})$	Signal (μ K) (noise)	$\chi^2 (df)$	Prob %
A2218				
source - ref (microK RJ):				
1	$1.2\mathrm{mm}$	1151. (712. 971.)	11.2 (6)	8.4
2	$2.1\mathrm{mm}$	80. (299. 342.)	7.9 (6)	24.8
4	$2.1\mathrm{mm}$ corr	39. (234. 207.)	4.7 (6)	58.1
ref2 - ref1 (microK RJ): _				
1	$1.2\mathrm{mm}$	3504. (1423. 2485.)	18.3 (6)	0.6
2	$2.1\mathrm{mm}$	2. (598.480.)	3.9 (6)	69.5
4	2.1 mm corr	-429. (467. 544.)	8.2 (6)	22.7
CL0016+16				
source - ref (microK RJ):				
1	$1.2\mathrm{mm}$	1. (172. 200.)	47.2 (35)	8.1
2	$2.1\mathrm{mm}$	-233. (118. 122.)	37.8 (35)	34.2
4	$2.1\mathrm{mm}$ corr	-384. (104. 109.)	38.2 (35)	32.5
ref2 - ref1 (microK RJ): $_$				
1	$1.2\mathrm{mm}$	243. (344. 464.)	63.6 (35)	0.2
2	$2.1\mathrm{mm}$	176. (235. 240.)	36.4 (35)	40.5
4	2.1 mm corr	-51. (209. 210.)	35.5 (35)	44.7

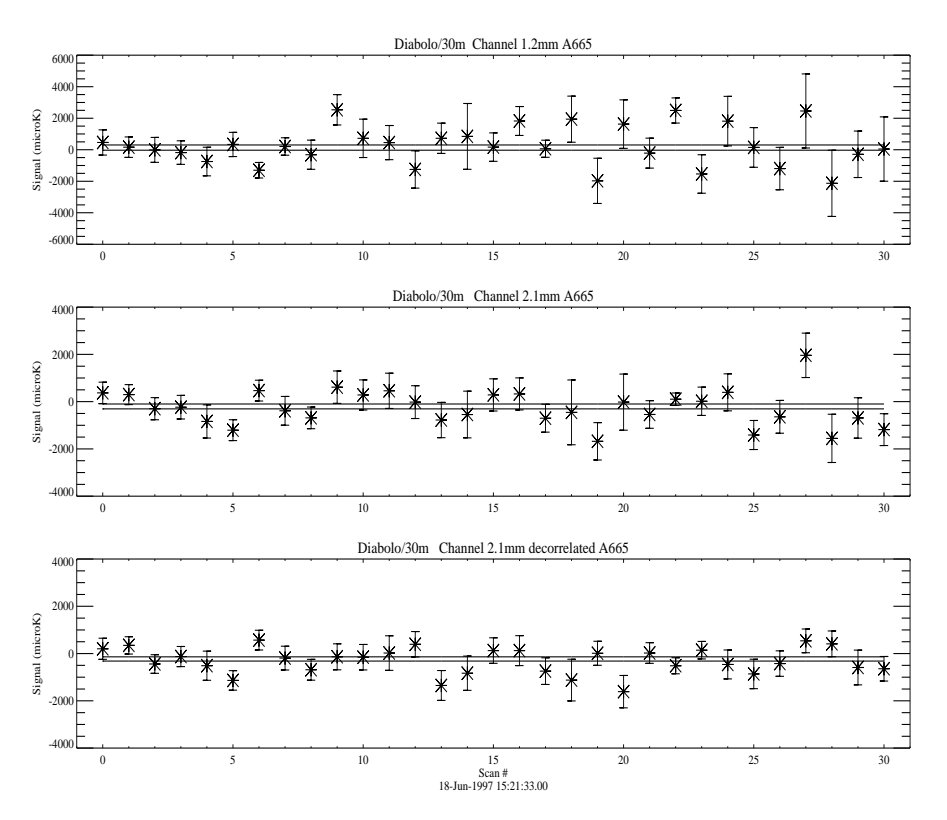


Fig. 6. Antenna temperature observed for cluster A665. The two upper plots show the two independent diabolo channel measurements and the lower plot is the the second channel corrected for atmospheric noise (see text). The 2 lines show $\pm 1\sigma$ from the final optimally averaged value.

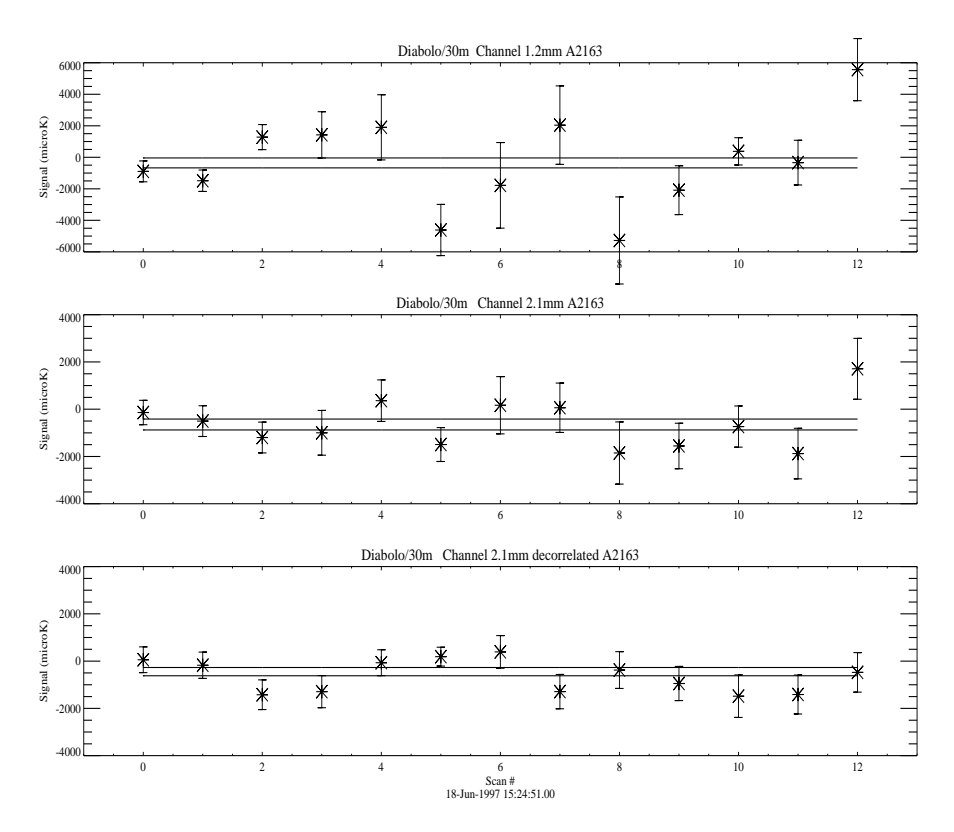


Fig. 7. Antenna temperature for the cluster A2163.

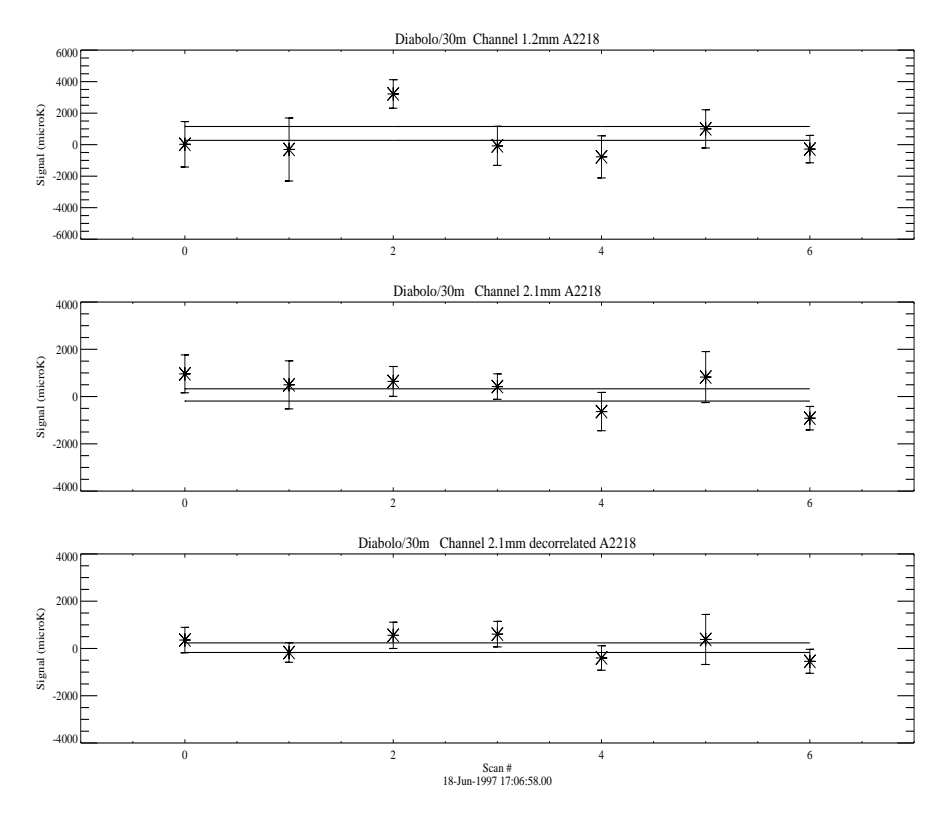


Fig. 8. Antenna temperature for the cluster A2218.

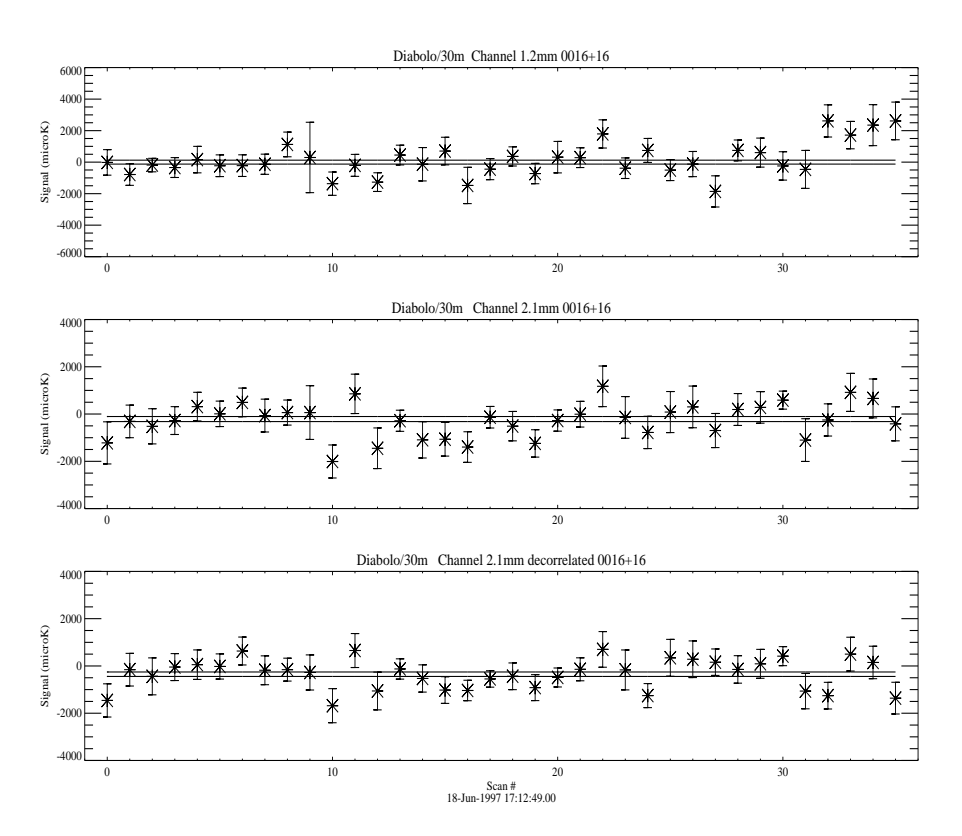


Fig. 9. Antenna temperature for the cluster CL0016+16.